A new instrument for the study of wave-particle interactions in space: One-chip Wave-Particle Interaction Analyzer

Hajime Fukuhara[1], Hirotsugu Kojima[2], Yoshikatsu Ueda[2], Yoshiharu Omura[2], Yuto Katoh[3], and Hiroshi Yamakawa[2]

[1]*Graduate School of Engineering, Kyoto University, Kyotodaigaku-katsura, Kyoto 615-8510, Japan*
[2]*Research Institute for Sustainable Humanosphere, Kyoto university, Gokasho, Uji, Kyoto 611-0011, Japan*
[3]*Planetary Plasma and Atmospheric Research Center, Graduate School of Science, Tohoku University, Sendai, Miyagi 980-8578, Japan*

Wave-particle interactions in a collisionless plasma have been analyzed in several past space science missions but direct and quantitative measurement of the interactions has not been conducted. We here introduce the Wave-Particle Interaction Analyzer (WPIA) to observe wave-particle interactions directly by calculating the inner product between the electric field of plasma waves and of plasma particles. The WPIA has four fundamental functions: waveform calibration, coordinate transformation, time correction, and interaction calculation. We demonstrate the feasibility of One-chip WPIA (O-WPIA) using a Field Programmable Gate Array (FPGA) as a test model for future science missions. The O-WPIA is capable of real-time processing with low power consumption. We validate the performance of the O-WPIA including determination of errors in the calibration and power consumption.
Key words: Wave-particle interaction, plasma waves, collisionless plasma, FPGA.

1. Introduction

Since space plasmas are essentially collisionless, their kinetic energies are altered mainly through wave-particle interactions. While plasma waves are destabilized by absorbing kinetic energy, the excited waves result in damping by energizing the plasma. Plasma wave receivers and plasma instruments on-board spacecraft take on the role of observing wave-particle interactions in space. Previous plasma wave receivers and plasma instruments were completely independent. In typical space missions, they were not controlled in coordinated ways and did not interact with each other. This independence made it difficult to quantitatively study wave-particle interactions. For example, direct correlation analyses using waveforms and velocity distribution functions were usually impossible by the difference in time resolutions.

Extensive attempts have been made in the past several decades to identify wave-particle interaction processes. There exist roughly two different methods for rocket or spacecraft observations. One is based on particle correlation techniques (Gough *et al.*, 1995; Gough, 1998). It calculates an autocorrelation (or cross-correlation) function using the particle detection pulses. Since the results depend on velocity modulations in the plasmas in phase space due to wave-particle interactions, they enable one to identify the energy source of plasma waves by comparing enhancements in the autocorrelation functions in different energy ranges with the plasma wave frequencies. Gough (1998) reported the auto correlation function had been modulated

with the upper hybrid frequency by an injection of electron beam into the ionosphere. Buckley *et al.* (2000) introduced an outline of the particle correlator for the Cluster mission and evidenced the capability of the correlator to detect wave particle interactions by simulation. Furthermore, the flight data of the particle correlator on board the Cluster spacecraft show the good correlation of the detected particle modulation frequencies with the frequencies of the observed plasma waves in the magnetosheath (Buckley *et al.*, 2001).

The other system is the so-called "Wave-Particle Correlator (WPC)" (Ergun *et al.*, 1991, 1998). The preceding correlator makes use of only the data from particle instruments, whereas the wave-particle correlator uses data from both plasma waves and particle instruments. It counts particle events detected by plasma instruments taking into account the phase observed by the plasma wave receivers. The advantage of this technique is it allows one to identify the direction of energy flow between plasma waves and plasmas, as well as to find out the wave energy sources. Kletzing *et al.* (2005) developed a new wave-particle correlator, which counts up detected particles according to phase divided into 16 bins. These wave-particle correlators showed the correlation between the phase of the Langmuir waves and the observed electron counts in the polar region. Of course, their technique can be applied to other waves in other regions.

In summary, the particle correlator provides autocorrelation functions, which are equivalent to the modulation frequency of plasmas in phase space, whereas the wave-particle correlator provides the number of particles detected during the period of a specific wave phase. In the present paper, we propose a new type of instrument with the capability to conduct direct and quantitative measurements of

wave-particle interactions. We name it the "Wave-Particle Interaction Analyzer (WPIA)." The WPIA quantifies the kinetic energy flow by the inner product of the amplitudes of the observed waves and velocities of the detected particles. The other methods do not consider all of the properties of the observed waveforms and particles. However, the WPIA considers instantaneous wave amplitudes and velocities of particles, as well as the phase relations between the waves and particles. Furthermore, since the wave-particle interactions are confined to specific directions relative to the ambient magnetic field, the WPIA also accounts for the direction of the ambient magnetic field in the above calculations. These calculations should be conducted on-board spacecraft since sending all of the data for the calculations needs a wide communication band of telemetry, which is actually not available.

The detailed principle of the WPIA is described in Section 2 and consists of complicated processes in its function. One of the easiest way to realize the WPIA is to develop software running on a digital processor on-board a spacecraft. However, the heavy load of the WPIA requires a dedicated processor on a real-time basis. This requirement does not always meet the capabilities of a spacecraft. Therefore, we have developed a Field Programmable Gate Array (FPGA) with all of the necessary functions of the WPIA. We call it the "One-chip Wave-Particle Interaction Analyzer (O-WPIA)." The O-WPIA realizes the capability of the WPIA with real-time processing and low-power consumption.

We submitted our proposal of the SCOPE (cross-Scale COupling in the Plasma universE) mission to JAXA (Japan Aerospace Exploration Agency) (SCOPE working group, 2008). The SCOPE targets the investigation of the cross-scale coupling in the terrestrial magnetosphere. If the proposal is approved, the SCOPE spacecraft will be launched in 2017. In this mission, since the wave-particle interaction is the key observational subject, we believe that the quantitative data of the O-WPIA will be exceedingly significant in this mission. On the other hand, we also join another proposal of the mission called "ERG (Energization and Radiation in Geospace)" (ERG working group, 2008). It is a small satellite mission, which focuses on the observation of the radiation belts of the Earth. In this mission, we propose the software-type WPIA (S-WPIA). In the S-WPIA, the functions and logics of the WPIA are realized by the software running on the on board general purpose processor. Since the S-WPIA does not have exclusive hardware, we cannot expect real-time operations of the WPIA. However, it is very efficient in the small satellite mission, in which the available resources of the satellite are very limited.

In this paper, we introduce the basic physical concept of the WPIA in Section 2. We also show the hardware logic of the WPIA installed in the one-chip FPGA in Section 3. After introduction of the hardware, we describe the test-design of the one-chip WPIA in Section 4. We evaluate the system operation, the errors, and the power consumption in the installed WPIA in Section 5. Finally, we summarize and conclude the paper in Section 6.

2.　Principle and Significance of the WPIA

The present section demonstrates the principle and significance of the WPIA by comparing it with the conventional methods used in earlier studies. In the conventional method for the study of wave-particle interactions using spacecraft observation data, one calculates the correlation of plasma wave data (such as frequency spectra) with plasma particle data (such as energy spectra). When attempting to identify physical mechanisms of plasma wave instabilities in detail, the reduced velocity distribution functions are examined in the periods of notable plasma wave activities. Since the correlation is visually examined in such methods, qualitative results are unavoidable. Moreover, one frequently faces a lack of time resolution in this conventional method. Since the energies of the particles fluctuate at a characteristic timescale in wave-particle interactions such as at an electron beam instability, the time resolution of the data should be high enough to trace the phenomenon.

An electron beam instability is a good example to demonstrate the advantage of the WPIA. Figure 1 schematically shows the relation between the velocity distribution (Fig. 1(a)) and phase space trajectories for beam particles (Fig. 1(b)) in the nonlinear stage. The vertical axis in Fig. 1(b) denotes the velocity component parallel to the ambient magnetic field, and the horizontal axis represents the phase relation of the particles and plasma waves (that is, the position of particles relative to the spatial structure of the electrostatic potentials). The center of the trajectories is aligned with the phase velocity (v_ϕ) of destabilized plasma waves. As the wave growth in the linear phase leads to the formation of an electrostatic potential, beam particles start getting trapped in the hatched region in Fig. 1(b) by losing their kinetic energies. The velocity width in the trapping region is defined by the trapping velocity (V_t),

$$V_t = 2\sqrt{\frac{eE_w}{m_0 k}} = 2\sqrt{\frac{ev_\phi E_w}{m_0 \omega_p}}, \qquad \left(\frac{\omega_p}{k} \sim v_\phi\right), \quad (1)$$

where E_w and ω_p are the wave amplitude and the electron plasma frequency, respectively. Once particles are trapped, their kinetic energies are exchanged with plasma wave energies, and the direction of energy flow (waves to particles or vice versa) is defined by the phase relation between the particles and plasma waves. A series of these processes results in the appearance of fluctuations with a width of $2V_t$ around v_ϕ in the reduced velocity distribution shown in Fig. 1(b). In conventional data processing for calculating velocity distributions, data integration of longer than a few seconds is necessary. This data integration process averages the fluctuations, resulting in the disappearance of the variations in the velocity distribution. Furthermore, despite the importance of the phase relation between the plasma waves and particles, the reduced velocity distribution loses the phase information.

The Japanese spacecraft Geotail succeeded in showing the importance of time domain observations of plasma waves, as realized by the Wave-Form Capture receiver (Matsumoto *et al.*, 1994a, b). It directly samples waveforms with an analog-digital converter of high sampling frequency. The time domain observations allow one to exam-

(a)
Observed velocity distribution

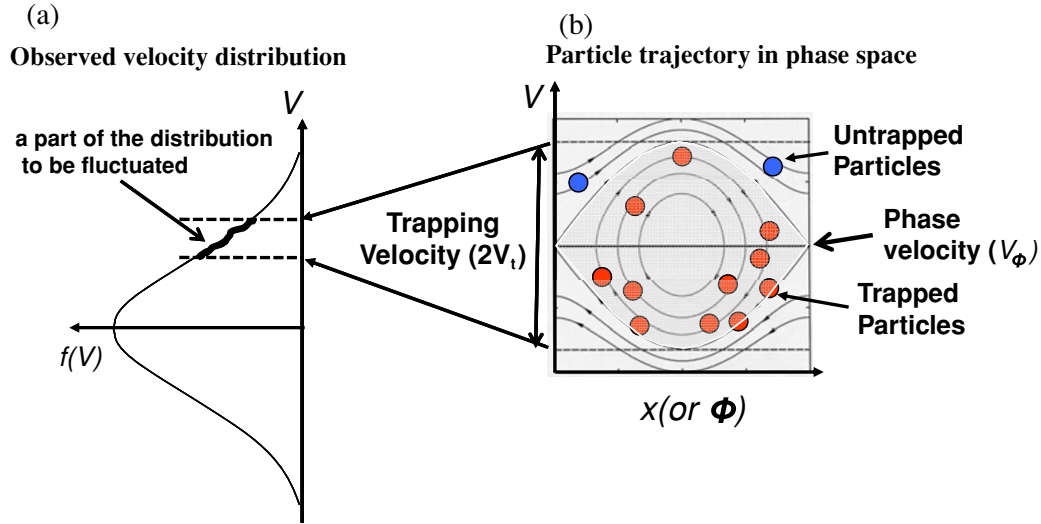
(b)
Particle trajectory in phase space

Fig. 1. Classical method in studying wave-particle interactions. The phase relation of the plasmas and plasma waves disappear in the reduced velocity distributions.

ine phase information of the waveforms. They also provide an opportunity to examine quick changes in wave features, because they do not require data accumulation, in contrast to the spectral analysis. On the other hand, high time resolutions in the velocity distribution measurements remain an important issue for future missions. The realization of superior plasma instruments with high time resolution is an excellent solution for quantitative research on wave-particle interactions in space plasmas. However, we believe that the WPIA provides another solution for future work. The WPIA measures an important physical quantity, $E_w \cdot v$, which quantitatively represents the wave-particle interaction, where E_w is the instantaneous electric field vector and v is the velocity vector of a plasma particle. Note that $E_w \cdot v$ is equivalent to a time variation in the kinetic energy of a single particle according to

$$\frac{d}{dt}\left(m_0 c^2 (\gamma - 1)\right) = q\, E_w \cdot v, \qquad (2)$$

where m_0, q, c, and γ denote the rest mass, charge of a particle, light speed, and Lorentz factor, respectively. The calculation of this physical value at the source region allows us to do quantitative studies of the wave-particle interaction. Since it is not enough to do the calculation for only one particle, we need some accumulation over a time period of at least several characteristic timescales in the target phenomenon as follows,

$$I = q \sum_i E_{w_i} \cdot v_i. \qquad (3)$$

Equation (3) is valid for the kinetic energy transfer in any wave-particle interaction process. The most significant difference between this method and the conventional one is that the data accumulation is conducted after considering the phase relation of E_w and v (see Fig. 2) as well as amplitude and velocities. Furthermore, the accumulation method is flexible. For example, we can examine the results with
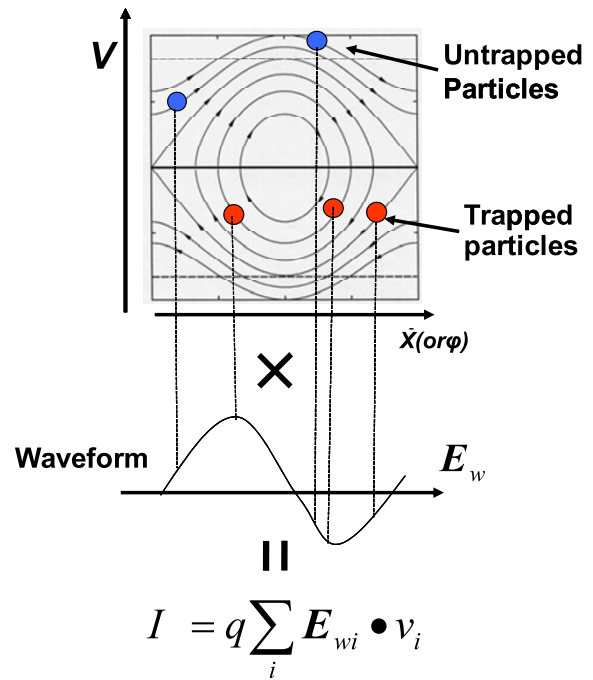

Fig. 2. Principle of the WPIA. The WPIA calculates $E_w \cdot v$ before accumulating the observed data.

fixed phase differences between the plasma waves and particles. In short, the main function of the WPIA is to calculate the physical quantity $E_w \cdot v$ and to accumulate it for a specific time period, i.e., the quantity "I" from Eq. (3), in various ways.

In order to calculate $E_w \cdot v$ without any integration or averaging processes, the WPIA simultaneously collects digitized waveforms picked up by a plasma wave receiver and pulses corresponding to the detection of plasma particles. Plasma wave observations and plasma measurements are essentially independent. However, the WPIA links these

two instruments and generates the physical quantity $E_w \cdot v$. While the waveform data are continuously input to the WPIA, output pulses with information on the arrival time and equivalent energy are impulsively input to the WPIA. The WPIA can also accumulate $E_w \cdot v$ in various ways.

Similar attempts to focus on the phase relation between the observed waves and timing of particle detection pulses have been conducted in previous rocket and satellite missions (Ergun *et al.*, 1991; Kletzing *et al.*, 2005). They counted up the number of particle detection pulses in reference to the phase of the observed Langmuir waves. In keeping the phase relation of waves and particles, their principle is similar to that of the WPIA. However, because they do not take into account the phase relation between the electric field vector and the particle velocity vector, their outputs are not quantitative physical values. In contrast, the WPIA provides $E_w \cdot v$, which is equivalent to the time variation of the kinetic energies. This is the significant and unique point of the WPIA compared with previous instruments.

The detailed inner processes of the WPIA are described in Section 3. The most important issue in realizing the WPIA is that it requires high-performance digital processing. For example, the WPIA needs the functions of FFT (Fast Fourier Transform) and IFFT (Inverse Fast Fourier Transform) as well as the calculation of $E_w \cdot v$. Since the WPIA needs to calibrate the observed waveforms before calculating $E_w \cdot v$, the FFT and IFFT processes are essential. The one-chip WPIA provides a solution for realizing a WPIA by keeping its mass and power consumption as small as possible.

3. Wave-Particle Interaction Analyzer (WPIA)
3.1 Interconnections with necessary sensors
In Section 2, we described the principle of the Wave-Particle Interaction Analyzer (WPIA) and stressed its advantage in studying wave-particle interactions via spacecraft observations. In conducting on-board calculations of energy exchanges among plasma particles and waves by the WPIA, it is indispensable to coordinate the plasma wave receivers with the plasma and magnetic field instruments. Figure 3 shows the interconnection of the WPIA with other sensors. Since the WPIA system calculates $E_w \cdot v$ on-board a spacecraft, it requires input of data from plasma sensors and fluxgate magnetometers as well as plasma wave sensors. Although scientific instruments on-board spacecraft are usually operated independently of other observation instruments, the WPIA works cooperatively with plasma wave, plasma, and magnetic field measurement instruments. Plasma wave receivers and plasma instruments transfer their observed data to the WPIA including their phase information. This means that plasma wave receivers and particle instruments should transmit the observed waveform data and the timing of the particle detection pulses with their energy information. Additional information such as the incoming directions of the detected particles are also sent to the WPIA. Further, the wave-particle interactions should be referred to the direction of the ambient magnetic field. For example, in the case of the interaction of electron beams and Langmuir waves, the calculation of $E_\parallel \cdot v_\parallel$ is essential, where $E_\parallel$ and $v_\parallel$ denote the instantaneous electric
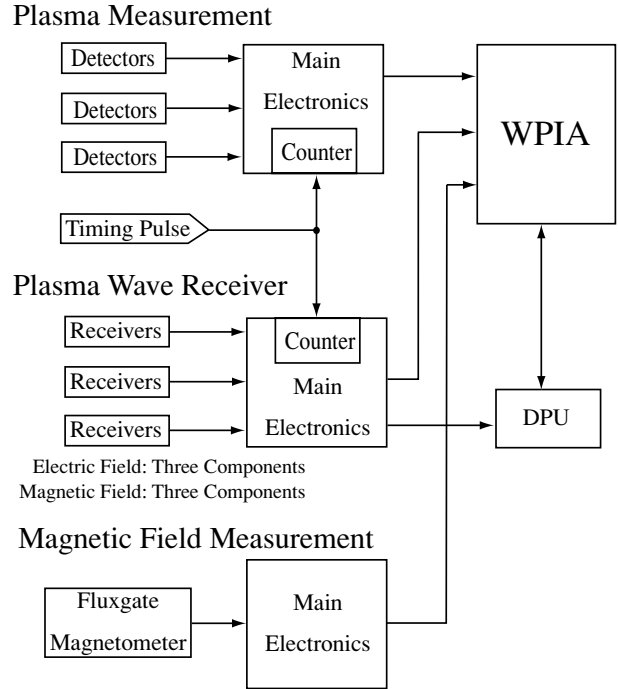

Fig. 3. Interconnection of the WPIA with other instruments.

field vector and the detected particle velocity vector relative to the ambient magnetic field, respectively. For this transformation of the coordinate system in wave vectors and velocity vectors of particles, the data of the fluxgate magnetometer are used. Real-time operation of the WPIA requires the data transmission line to have a large enough capacity to send all of the data without any delays to the WPIA. If the system cannot provide enough data transmission capacity to the WPIA, some data buffers for storing the observed waveforms and particle information should be prepared. In that case, it is difficult to guarantee the real-time calculation of $E \cdot v$.

3.2 Blocks to be implemented
Figure 4 shows a block diagram of the WPIA. It describes the necessary functions to be implemented in the WPIA. As already mentioned, knowing the precise phase relation between the waveforms and the timing of the pulses is very important. Therefore, waveform calibration and data conversion such as transformation of the coordinate system are essential functions of the WPIA. In addition, as particle data are asynchronously obtained with respect to waveform data, we need information on their relative time difference to calculate $E_w \cdot v$ accurately.

Because the characteristics of wave receivers and sensors affect the amplitude and phase of the observed waveform, we need to calibrate the waveforms. The "Waveform Calibration" block shown in Fig. 4 takes the role of canceling the effects of analog circuits and sensors. The importance of the phase relation between the observed electric field vector and particle velocity vector is stressed. It is essential to obtain calibrated phase in the WPIA. The calibration is conducted by the FFT ($\mathcal{F}$) and IFFT ($\mathcal{F}^{-1}$) calculations using the calibration values of the plasma wave receivers and
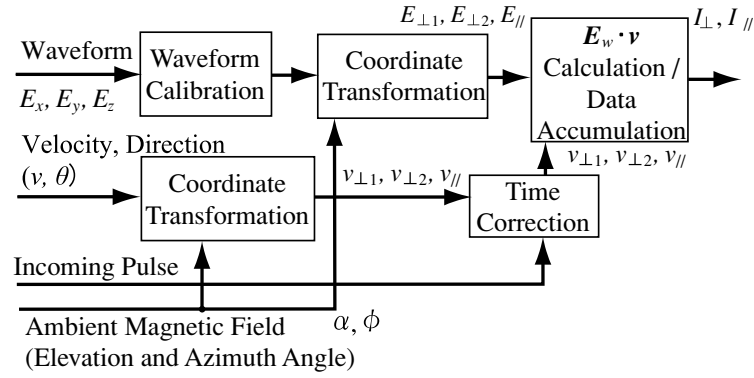
Fig. 4. Data flow diagram of the WPIA.

sensors,

$$X(f) = \mathcal{F}[x(t)], \tag{4}$$

$$x_{\text{cal}}(t) = \mathcal{F}^{-1}\left[G^{-1}(f)X(f)\right], \tag{5}$$

where $x(t)$ denotes a time series of sampled raw wave-form data, $G(f)$ is the transfer function of the plasma wave receiver including its sensor characteristics measured in ground tests, and $x_{\text{cal}}(t)$ is the time series data of calibrated waveforms. This calibration process should be applied to each component of a waveform. When the plasma wave receiver observes six components of waveforms simultaneously (i.e., three components for electric fields and three components for magnetic fields), six calibration processes will run on the WPIA in parallel. Thus, the calibration process causes the heaviest load on the WPIA. In the SCOPE mission including the one-chip type of the WPIA, satellites are spin-stabilized and have short rigid electric antennas along the satellite spin axis. Though the sensitivity of the short rigid antenna is generally much worse than a long wire antenna deployed perpendicular to the spin axis, the spin-axis antenna will have enough sensitivity for observing target plasma waves because of the low noise preamplifier. Therefore, there is a difference of characteristics between the spin-axis antenna and wire antennas. The WPIA can calibrate waveforms using the independent calibration data for each axis of the antennas to provide measurements of the three components of the electric field with good precision.

The physical properties of the wave-particle interactions should be referenced to the local ambient magnetic field direction. The "Coordinate Transformation" block transforms the observed waveforms and particles relative to the ambient magnetic field. Figure 5 shows a typical coordinate system in a spin-stabilized spacecraft. $\boldsymbol{B}$ in Fig. 5 is the local ambient magnetic field vector. The transform matrix is given by

$$\boldsymbol{r}_{\text{LM}} = \left[\hat{\alpha}\right]\left[\hat{\phi}\right]\boldsymbol{r}_{\text{SC}},$$

$$\boldsymbol{r}_{\text{LM}} = \left(r_{\perp 1}, r_{\perp 2}, r_{\parallel}\right)^T, \quad \boldsymbol{r}_{\text{SC}} = \left(r_x, r_y, r_z\right)^T, \tag{6}$$

$$\left[\hat{\phi}\right] = \begin{pmatrix} \cos\phi & \sin\phi & 0 \\ -\sin\phi & \cos\phi & 0 \\ 0 & 0 & 1 \end{pmatrix}, \left[\hat{\alpha}\right] = \begin{pmatrix} \cos\alpha & 0 & -\sin\alpha \\ 0 & 1 & 0 \\ \sin\alpha & 0 & \cos\alpha \end{pmatrix},$$
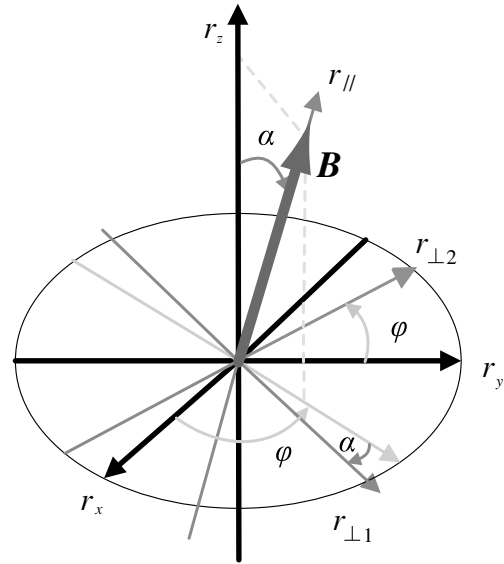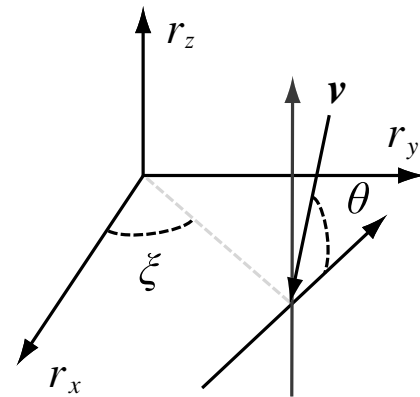

Fig. 5. Relation between the coordinate system of the spacecraft and the ambient magnetic field.

Fig. 6. Relation between the coordinate system of the spacecraft and the coordinate system of a particle detector on a spacecraft which has a constant angle ξ relative to the r_x-axis. A particle with velocity v comes from a direction at angle θ to the $r_x r_y$-plane.
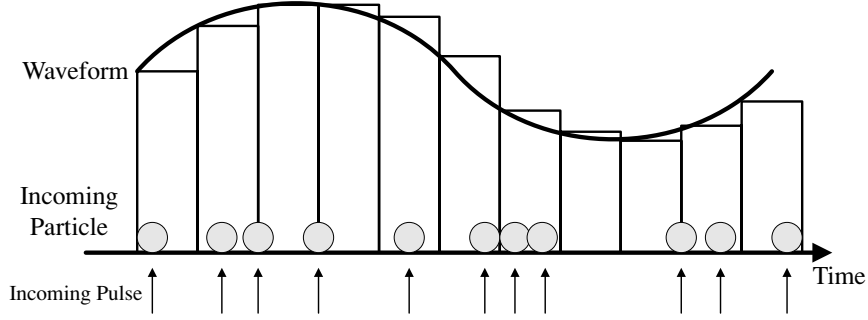
Fig. 7. Schematic illustration indicating that a waveform is sampled and held at a sampling frequency although the particles are asynchronously caught by the particle detector.

where r_{LM} and r_{SC} are given vectors fixed in the local magnetic coordinate system and in the spacecraft coordinate system, respectively. Both suffixes 'LM' and 'SC' are appended to electric field vector E, and particle velocity vector v in this paper. In the local ambient magnetic field coordinate system, $\perp 1$ and $\perp 2$ are two orthogonal components in the plane perpendicular to the ambient magnetic field, $\parallel$ means the direction parallel to the magnetic field B, ϕ and α are an azimuth and elevation angle, respectively.

Moreover, since plasma sensors are independently located in different positions on the spacecraft, we need another transformation calculation. If we obtain particle data as shown in Fig. 6, the transformation for particle data is given by Eq. (7), where ξ is the constant angle between the particle sensor and the r_x-axis of the spacecraft coordinate system,

$$
\begin{aligned}
v_{\text{SC}} &= \left(v_x, v_y, v_z\right)^T \\
&= v \begin{pmatrix} \cos\xi & -\sin\xi & 0 \\ \sin\xi & \cos\xi & 0 \\ 0 & 0 & 1 \end{pmatrix} \begin{pmatrix} 0 \\ \cos\theta \\ \sin\theta \end{pmatrix} = \begin{pmatrix} -v\sin\xi\cos\theta \\ v\cos\xi\cos\theta \\ v\sin\theta \end{pmatrix}.
\end{aligned}
\tag{7}
$$

The timing of particle detection pulses is not synchronized with the sampled waveforms of the plasma waves. The "Time Correction" block corrects the time difference in the observations of the waveforms and incoming particle pulses as shown in Fig. 7. To conduct the time correction, we need to know the precise relative time difference. The "Time Correction" block works as a controller to calculate $E_{\text{w}} \cdot v$ with enough accuracy in view of the relative time difference.

The "$E_{\text{w}} \cdot v$ Calculation/Data accumulation" block calculates $E_{\text{w}} \cdot v$ and sums up the results in the parallel and perpendicular directions relative to the ambient magnetic field,

$$
\tilde{I}_\perp = E_{\perp 1} v_{\perp 1} + E_{\perp 2} v_{\perp 2}, \tag{8}
$$

$$
\tilde{I}_\parallel = E_\parallel v_\parallel, \tag{9}
$$

where $\tilde{I}_\perp$ and $\tilde{I}_\parallel$ are the perpendicular and parallel components relative to the magnetic field, respectively, $E_{\perp 1}$, $E_{\perp 2}$, $v_{\perp 1}$, $v_{\perp 2}$ are the electric fields and particle velocities in the perpendicular directions, and $E_\parallel$, $v_\parallel$ are the

parallel components. Furthermore, "$E_{\text{w}} \cdot v$ Calculation" accumulates $\tilde{I}_\perp$ and $\tilde{I}_\parallel$ to detect the wave-particle interactions,

$$
I_\perp = \sum \tilde{I}_\perp = \sum \left(E_{\perp 1} v_{\perp 1} + E_{\perp 2} v_{\perp 2}\right), \tag{10}
$$

$$
I_\parallel = \sum \tilde{I}_\parallel = \sum E_\parallel v_\parallel. \tag{11}
$$

The accumulated values of $I_\perp$ and $I_\parallel$ are obtained as the physical measure of the wave-particle interactions.

4. One-chip WPIA
4.1 Advantages of the One-chip WPIA

The fundamental functions and interconnections of the WPIA with other sensors were described in Section 3. The major functions of the WPIA can be realized by software running on a high-performance Central Processing Unit (CPU) or Digital Signal Processor (DSP). However, almost every computational resource of CPU or DSP is assigned to the WPIA due to the heavy load in the waveform calibrations and management of the data transfer from other sensors. We propose a one-chip WPIA as a solution for this difficulty. The one-chip WPIA possesses all of the necessary functions described in Section 3. All of the functions are installed in the Field Programmable Gate Array (FPGA). The one-chip WPIA has such advantages as real-time processing and low power consumption.

Figure 8 shows an evaluation board used in the development of the one-chip WPIA. It contains three channels of plasma wave receivers, input channels of the magnetic field and plasma instruments, as well as the FPGA. The three channels of plasma wave receivers collect waveforms at a sampling frequency of 62.5 kHz and transfer the waveform data with 16 bits to the WPIA through First-In First-Out (FIFO) memories. The frequency range to be observed in the plasma wave receivers is assumed to be from several hundred Hz to around a dozen kHz in the SCOPE mission. Therefore the O-WPIA is expected to observe wave particle interactions involving plasma waves such as whistler-mode chorus, Langmuir wave, or etc. which have a frequency of less than a dozen kHz. These specifications of the plasma wave receivers are almost the same as those of typical ones for targeting observations in the terrestrial magnetosphere.

A top-hat type particle detector utilizing the spacecraft spin will be installed in the mission. Although the field of view of the particle detector is limited in a very short time
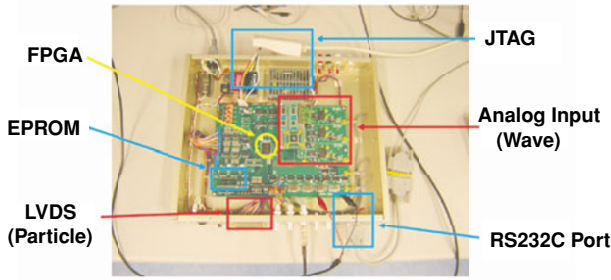
Fig. 8. Evaluation board for developing the one-chip WPIA. It contains the FPGA device (located in the center of the figure) and peripheral circuits including simple plasma wave receivers and simulators of plasma and magnetic field sensors.

Table 1. Logic cells of Virtex-II XC2V1000 FG456.

Function	Number
Logic Cells	11,520
Block Select RAM (kb)	720
18×18 Multipliers	40
Digital Clock Management Blocks	8
Max Dist RAM (kb)	160
Max Available User I/O	432

duration, the phase of the observed waves in the frequency range from several hundreds of Hz to several kHz rotates much faster than the spacecraft spin velocity. This means the O-WPIA can accumulate a lot of data on the phase relation of $E_w \cdot v$ even if the phase resolution of the particle detector is coarse. Thus, it can keep enough signal-to-noise ratio with limitation of the field of view.

We adopt the FPGA of the XILINX XC2V1000 with 1 million gates. The operational clock frequency can be selected with an on-board switch as 1.920, 4.096, 40, or 100 MHz or by the external optional clock signal. In the present paper, we set the clock frequency to 4 MHz by feeding in an external clock signal. Constant values such as the calibration data of the waveforms can be loaded onto the FPGA from the Erasable Programmable Read-Only Memory (EPROM) installed on the evaluation board. Detailed specifications of the FPGA applied to the one-chip WPIA are summarized in Table 1.

4.2 Design of the One-chip WPIA

4.2.1 Waveform Calibration Figure 9 shows the state transition diagram of the "Waveform Calibration" block. As mentioned in Section 3, we make use of the FFT and IFFT functions in the "Waveform Calibration" block. The transforms are implemented as complex FFT and IFFT which can concurrently transform two components of waveforms by inputting two data sets into their real and imaginary parts. Therefore, two pairs of FFT and IFFT blocks are enough to conduct the calibration of three components of waveforms at once. We show a block diagram of the "Waveform Calibration" in Fig. 10. The forward FFT blocks read the sampled raw waveforms from the FIFOs of the plasma wave receiver and obtain the results of the FFT correspond-
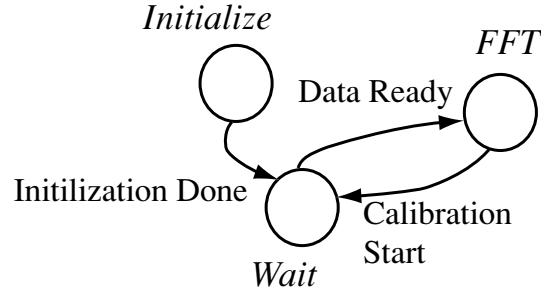

Fig. 9. State transition diagram of the "Waveform Calibration" block.

ing to $X(f)$ in Eq. (4). The multipliers calculate the product of the results of the FFT and calibration data which are loaded from the on-board EPROM into Block Select RAM memory (inside the FPGA) at the initialization stage of the system. The inverse FFT block calculates the inverse transform of the product and outputs the calibrated waveforms. The calibrated waveforms are stored in FIFOs on the FPGA and read out the sampling frequency at the next block.

In the FFT, the discrete frequency is

$$f_k = \frac{f_s}{L}k \quad (k = 0, 1, 2, \cdots L - 1), \tag{12}$$

where L is the number of sampled data points and f_s is the sampling frequency, respectively. Note that $X(k)$ is symmetrical, as indicated by Eqs. (14) and (15),

$$X(k) = \sum_{n=0}^{L-1} x(n)e^{-j\frac{2\pi k}{L}n}, \quad (n = 0, 1, 2, \cdots L - 1) \tag{13}$$

$$\mathrm{Re}\left[X(L - k)\right] = \mathrm{Re}\left[X(k)\right], \tag{14}$$

$$\mathrm{Im}\left[X(L - k)\right] = -\mathrm{Im}\left[X(k)\right], \tag{15}$$

where $X(k)$ can be obtained from $X(0)$ to $X(L-1)$ sequentially and is multiplied by $H(k)$ which is the calibration data given by

$$H(k) = G^{-1}(f)\big|_{f=f_k} = \frac{e^{-j\varphi(f_k)}}{A(f_k)}, \tag{16}$$

$$= \begin{cases} H_{\mathrm{real}}(k) + jH_{\mathrm{imag}}(k) \\ \quad (0 \le k < L/2 - 1) \\ H_{\mathrm{real}}(L - k) - jH_{\mathrm{imag}}(L - k) \\ \quad (L/2 \le k < L - 1), \end{cases} \tag{17}$$

where $A(f_k)$, and $e^{-j\varphi(f_k)}$ denote the calibration data of the plasma wave receiver in gain and phase, respectively. The calibrated waveform $x_{\mathrm{cal}}(n)$ is obtained from the following IFFT,

$$x_{\mathrm{cal}}(n) = \frac{1}{L}\sum_{k=0}^{L-1} H(k)X(k)e^{j\frac{2\pi n}{L}k}. \tag{18}$$

The sampled waveform data are transmitted to the one-chip WPIA through the FIFO with a capacity of 4096 words. Since a series of data is continuously input to the forward FFT at the clock frequency, we need to choose L to be less than or equal to 4096 to avoid overflow of the
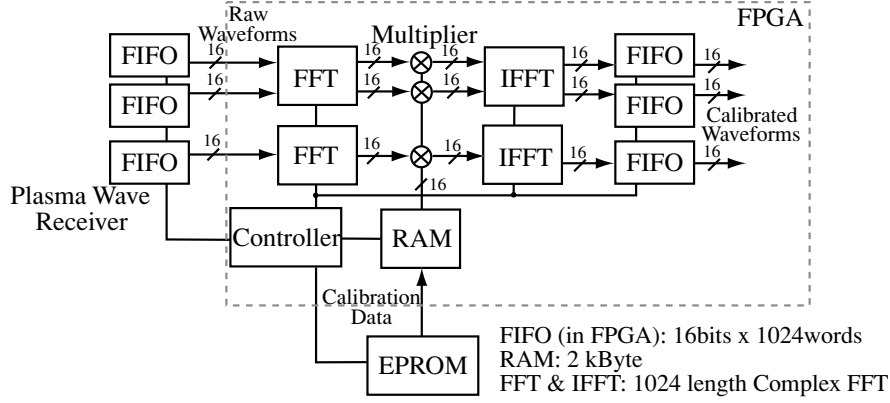
FIFO (in FPGA): 16bits x 1024words
RAM: 2 kByte
FFT & IFFT: 1024 length Complex FFT

Fig. 10. Block diagram of the "Waveform Calibration".

FIFO. The number of data L affects the frequency resolution as well as the processing time (equivalent to the time resolution). We need to choose it by considering the target phenomena from the point of view of frequency and time resolution. We also need to take into account the available logic gates of the FPGA in determining L. In this paper, L is fixed at 1024, which is equivalent to a frequency resolution of 61 Hz.

Since the load of the FFT calculations is the heaviest in the one-chip WPIA system, an estimation of the processing time of the FFT including the coordinate transformation is important. The period (T_{in}) required to obtain the waveforms depends on the number of data L. Further, the period to calculate the forward and inverse FFTs (T_{cal}) also depends on L. The "Coordinate Transformation" block processes the data in T_{trans} equivalent to three cycles of the system clock. Thus, the total time (T_{total}) can be estimated as the sum of T_{in}, T_{cal}, and T_{trans}. The particle data to be processed with the waveform data are kept in the Block Select RAM during the period of T_{total} in order to make it possible to conduct a series of calculations without delay. These periods are given by

$$T_{in} = \frac{L}{f_s}, \tag{19}$$

$$T_{cal} = \frac{N_{cal}}{f_c}, \tag{20}$$

$$T_{trans} = \frac{N_{trans}}{f_c} = \frac{3}{f_c}, \tag{21}$$

$$T_{total} = T_{in} + T_{cal} + T_{trans},$$
$$= \frac{L}{f_s} + \frac{N_{cal} + 3}{f_c}, \tag{22}$$

where $f_s = 62.5$ kHz is the sampling frequency, $f_c = 4$ MHz is the clock frequency of the FPGA, and N_{cal} and N_{trans} are the number of clock cycles of calibration and coordinate transformation, respectively. In the case of $L = 1024$, $N_{cal} = 12542$ cycles are needed to complete the whole calibration process (data load and transformation: 6264 cycles/FFT, delay to output: 7 cycles/FFT; determined by specification of applied Intellectual Property (IP) core). Thus, the period and number of clock cycles are calculated to be

$$T_{in} = 16.384 \text{ ms}, \tag{23}$$

$$T_{cal} = 3.1355 \text{ ms}, \tag{24}$$

$$T_{trans} = 0.75 \text{ } \mu\text{s}, \tag{25}$$

$$T_{total} = 19.52025 \text{ ms}, \tag{26}$$

$$N_{total} = f_c T_{total} = 78081 \text{ cycles}. \tag{27}$$

Equation (27) implies that the calibrated waveforms are obtained after 78081 clock cycles.

The count rate of the plasma detectors should also be considered in the design of the one-chip WPIA. It strongly depends on the plasma flux and on the sensitivity of the plasma sensors. In our current design of the one-chip WPIA, we assume the maximum count rate is expected to be 10^5/s in the SCOPE mission along its orbit inside the magnetosphere. Therefore the expected number of particle count pulses for the period of $T_{total} = 19.52025$ ms is 1952. The bit width of the Block Select RAMs for particle data is 65, since we need to store 16-bit velocity data for particles in three dimensions and 17-bit time information at which each particle is detected. In considering the amount of RAM to keep the particle data, we must set L to be less than or equal to 1024.

4.2.2 Coordinate Transformation   The "Coordinate Transformation" blocks calculate the parallel and perpendicular components of the waves and velocities of the particles in reference to the ambient magnetic field,

$$\boldsymbol{E}_{LM} = [\hat{\alpha}][\hat{\phi}]\boldsymbol{E}_{SC} \tag{28}$$

$$\boldsymbol{v}_{LM} = [\hat{\alpha}][\hat{\phi}]\boldsymbol{v}_{SC}, \tag{29}$$

where $\boldsymbol{E}_{LM} = (E_{\perp 1}, E_{\perp 2}, E_{\parallel})^T$, $\boldsymbol{E}_{SC} = (E_x, E_y, E_z)^T$, $\boldsymbol{v}_{LM} = (v_{\perp 1}, v_{\perp 2}, v_{\parallel})^T$, and $\boldsymbol{v}_{SC} = (v_x, v_y, v_z)^T$.

It is necessary to calculate the product of the two matrices $[\hat{\alpha}]$ and $[\hat{\phi}]$. The number of available multipliers are limited and the multiplication needs two clock cycles at least in the FPGA because of specification of applied multipliers. To decrease them, the one-chip WPIA calculates the multiplication by one matrix, as shown in Eqs. (30), (31), and (32). The diagram in Fig. 11 shows the operation of the
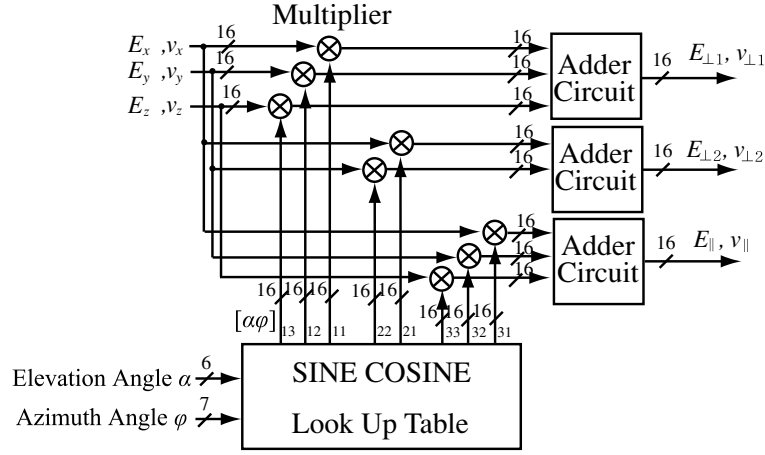
Fig. 11. Block diagram of the "Coordinate Transformation" for the ambient magnetic field coordinate system.
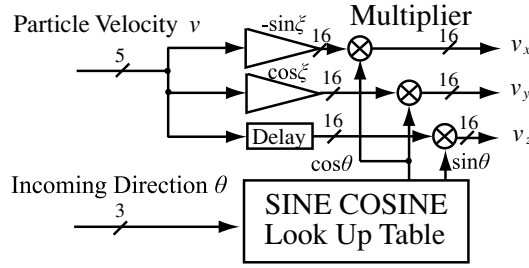

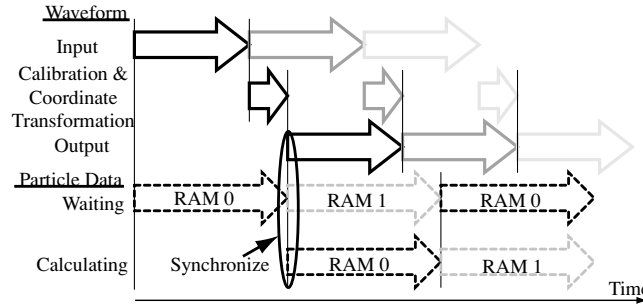Fig. 12. Block diagram of the "Coordinate Transformation" for the spacecraft coordinate system.

Fig. 13.   Timing chart for the time correction. After the first input of waveform data, calculations of the waveform calibration and coordinate transformation start while the second input starts. The first particle data set is written in RAM0 and waits for the end of the calculations of the first waveform data set. When the calculations are finished, RAM0 transfers the first data set and RAM1 takes the role of RAM0.

multiplication,

$$\boldsymbol{E}_{\text{LM}} = [\hat{\alpha\phi}]\boldsymbol{E}_{\text{SC}}, \tag{30}$$

$$\boldsymbol{v}_{\text{LM}} = [\hat{\alpha\phi}]\boldsymbol{v}_{\text{SC}}, \tag{31}$$

$$[\hat{\alpha\phi}] = \begin{pmatrix} \frac{\cos(\alpha+\phi)+\cos(\alpha-\phi)}{2} & \frac{\sin(\alpha+\phi)-\sin(\alpha-\phi)}{2} & \sin\alpha \\ -\sin\phi & \cos\phi & 0 \\ \frac{\sin(\alpha+\phi)+\sin(\alpha-\phi)}{2} & \frac{-\cos(\alpha+\phi)+\cos(\alpha-\phi)}{2} & \cos\alpha \end{pmatrix}, \tag{32}$$

where $\sin\alpha$, $\cos\alpha$, $\sin\phi$, $\cos\phi$, $\sin(\alpha + \phi)$, $\cos(\alpha + \phi)$, $\sin(\alpha - \phi)$, and $\cos(\alpha - \phi)$ are obtained from sine and cosine lookup tables.

The "Coordinate Transformation" needs three clock cycles. Two clock cycles are necessary for the multiplication and one clock cycle is necessary for loading the values from the tables.

The design of the "Coordinate Transformation" block for the spacecraft coordinate system is shown in Fig. 12. This block transforms the speed of a particle and its incoming direction into the velocities (v_x, v_y, v_z) before the other transformation is performed.

4.2.3 Time Correction The waveforms and particle data are asynchronously obtained. Moreover, the particle data must wait for the end of the "Wave Calibration" and "Coordinate Transformation" processes as shown in
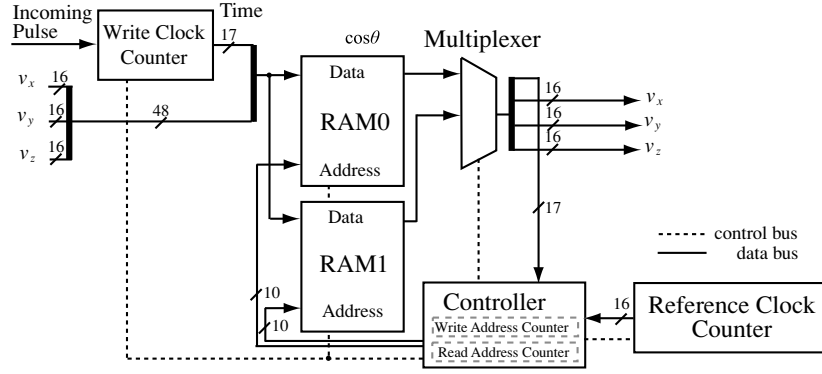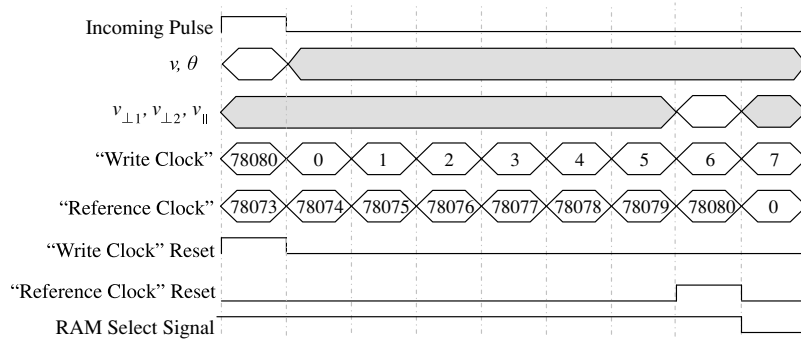
Fig. 14. Block diagram of the "Time Correction".

Fig. 15. Data v and θ are captured when the incoming pulse becomes 'High'. It takes seven clock cycles to transform v and θ into $v_{\perp 1}$, $v_{\perp 2}$, and $v_{\parallel}$. The incoming pulse is held in seven clock cycles to save information about time. Thus the "Reference Clock" is reset and the RAM select signal is inverted seven clock cycles behind the reset of the "Write Clock".

Fig. 13. The "Time Correction" is a controller that synchronizes the waveform and particle data, as sketched in Fig. 14.

In the "Time Correction" block, the one-chip WPIA has two clock counters, which indicate the relative time difference of the sampled waveforms and the detected plasma pulses. Both counters count at the clock frequency of the FPGA. One of the clocks is called the "Write Clock" and the other is the "Reference Clock." While the "Write Clock" starts counting when the sampling of the raw waveforms starts, the "Reference Clock" begins when the first calibrated waveforms are generated. The "Write Clock" and "Reference Clock" are reset to zero if the count of each clock reaches N_{total} of 78081 clock cycles. Since two Block Select RAMs are prepared inside the FPGA, they are switched between reading and writing by so-called switching buffers. Both RAMs have individual address counters and they are reset to zero when the RAMs are switched. The transformation for the particle data needs seven clock cycles (load trigonometric function values: 2 cycles, twice multiplication: 2×2 cycles, hold sum of the products, 1 cycles). The "Reference Clock" is reset every seven clock cycles behind the reset of the "Write Clock" to synchronize accurately, as shown in Fig. 15. When an incoming pulse from the plasma instruments is detected, the count number of the "Write Clock" is held in a temporary memory and the address counter of the writing RAM process is incremented.

The held count is stored again with the transformed velocity ($v_{\perp 1}$, $v_{\perp 2}$, $v_{\parallel}$), in the area which the writing RAM address indicates. After switching the roles of the RAMs, the stored count is compared with the "Reference Clock" count. If the stored count and the "Reference Clock" are equal to each other, the stored velocity is read out from the RAM and the RAM address is incremented. We can thereby obtain synchronized particle data with calibrated waveforms and calculate $E_{\text{w}} \cdot v$.

4.3 Calculation of $E_{\text{w}} \cdot v$/Accumulation

In the "Calculation of $E_{\text{w}} \cdot v$/Accumulation" block, $I_{\perp}$, and $I_{\parallel}$ are calculated and accumulated for a given period represented by Eqs. (10) and (11). The accumulation time depends on the required time resolution. The amount of time needed to accumulate $I_{\parallel}$ and $I_{\perp}$ should be a few times larger than one period of the observed waves since we should consider phase relation between the plasma waves and particles for various phases of the plasma waves. The frequency of observed plasma waves is assumed to be less than a dozen kHz in the SCOPE mission. In this study, we use a period of 64 times the $E_{\text{w}} \cdot v$ calculation. Assuming a particle count rate of 10^5/s, the time resolution is 640 μs. This value is sufficient since it is equal to a few times larger than one period of the waves.

The design of the "Calculation of $E_{\text{w}} \cdot v$" block is shown in Fig. 16. Three multipliers independently calculate the product of the electric field and the particle velocity,
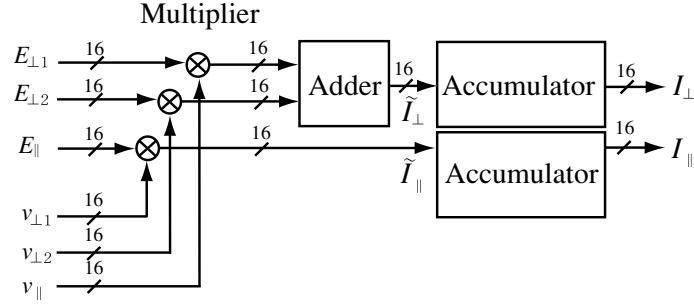
Fig. 16. Block diagram of the "$E_\mathrm{w} \cdot v$ Calculation".
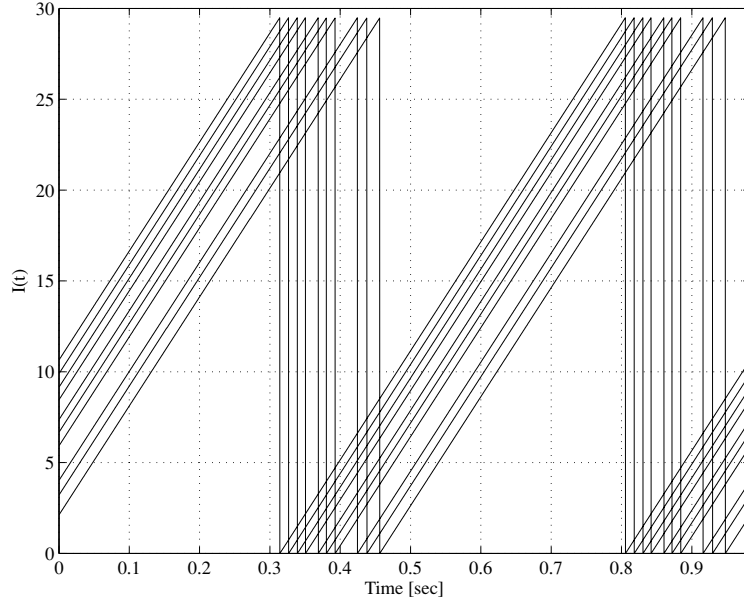
Fig. 17. Ten results of $I(t) = \sum E(t) \cdot v(t)$. There is only a time distinction between the curves.

$E_{\perp 1}v_{\perp 1}$, $E_{\perp 2}v_{\perp 2}$, and $E_{\parallel}v_{\parallel}$. Products in two perpendicular directions ($E_{\perp 1}v_{\perp 1}$ and $E_{\perp 2}v_{\perp 2}$) are added before accumulation. The calculations of $\tilde{I}_\perp$ and $\tilde{I}_\parallel$ are held in two separate accumulators. The multipliers are enabled every time that particle data are read out from the "Time Correction" and the accumulators are enabled two clock cycles later.

5. Performance

In this section, we demonstrate that the one-chip WPIA properly functions on the FPGA. We also estimate the power consumption of the one-chip WPIA with application to future missions in mind.

5.1 Operational accuracy

We checked the one-chip WPIA functions by giving it $E(t)$ and $v(t)$ dummy data, which are time series of electric field and particle velocity vectors, respectively. In order to make it easy to examine the functions, we use the following simple dummy data,

$$E(t) = (E_0 \sin(2\pi f t + \varphi), 0, 0)^T, \tag{33}$$

$$v(t) = \left(v_0 \sum_k \delta\left(t - \frac{k}{f_\mathrm{v}}\right), 0, 0 \right)^T. \tag{34}$$

Here E is a sinusoidal wave with frequency f, and v is a series of periodic pulses at a cycle of $1/f_\mathrm{v}$ expressed as a sum of delta functions, respectively. Both E and v are generated within the FPGA.

Assuming the ratio of f/f_v is equal to an integer, the output of the one-chip WPIA should be

$$I(t) \propto t. \tag{35}$$

By using these dummy data, we can confirm the functions of the whole one-chip WPIA including the "Waveform Calibration", "Time Correction", "Coordinate Transformation", and "Calculation of $E_\mathrm{w} \cdot v$."

Figure 17 shows the output $I(t)$ of the one-chip WPIA for the above check configuration. Both of the frequencies f and f_v are set to 3.90625 kHz, which is equal to exactly $1/16$ of the sampling frequency of the wave receiver. The output $I(t)$ is reset every 524 ms in order to avoid overflow of the accumulators in the "Calculation of $E_\mathrm{w} \cdot v$." The results show that the output is proportional to the time step number without distortions, and therefore the one-chip WPIA on the FPGA operates as designed. Notably it is confirmed that the functions of the time correction and the
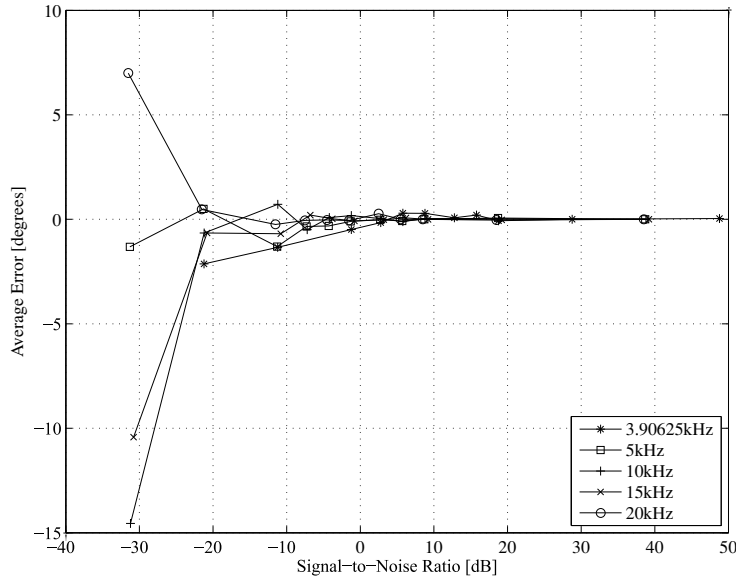
Fig. 18.   Average errors in the "Waveform Calibration" are plotted against the signal-to-noise ratio at the frequencies of the input waveform of
3.90625 kHz, 5 kHz, 10 kHz, 15 kHz, and 20 kHz.

calculation of $E_w \cdot v$ work properly.

5.2   Calibration errors

The phase of the collected waveforms are important in calculating $E_w \cdot v$. We therefore need to evaluate the expected phase errors depending on the signal-to-noise-ratio (SNR). To do so, we measure the errors in the "Waveform Calibration" to examine the influence of noise.

The errors in the "Waveform Calibration" are measured as follows:

1. A sinusoidal waveform with a fixed frequency is fed to the plasma wave receiver on the evaluation board.
2. The digitized waveform from the A/D converter is input to the one-chip WPIA through the FIFO.
3. The waveforms at the input and output of the "Waveform Calibration" block are transfered to the workstation through the Joint Test Action Group (JTAG) cable.
4. The phase errors are measured by comparing the phases of the input and output waveforms on the workstation.

In these measurements, we make use of the calibration table in the whole frequency range at a gain of 0 dB and phase of 90°. The frequencies are 5 kHz, 10 kHz, 15 kHz, 20 kHz, and 3.90625 kHz ($= f_s/16$), which is chosen to investigate the influence of the discretization. The measurements are conducted twenty times under the same conditions except for the initial phase of the raw waveforms. The average and standard deviation are calculated at each frequency.

In Figs. 18 and 19, these errors are plotted versus the SNR, at the indicated frequencies. The average errors are larger than 0 dB at small SNR because of the increased noise. The standard deviation of the errors becomes large when the SNR is smaller than 10 dB. Furthermore, at low frequency the standard deviation increases. The relative difference between the true frequency of the raw waveform and the discrete frequency of the calibrated waveforms is not related to the increase in the standard deviation at 3.90625 kHz. Therefore, since the waveform period in a fixed length FFT decreases with decreasing frequency, the larger standard deviation is caused by the growing data spread due to the difference in the initial phase of the waveform.

In general, the angular resolution of a plasma detector is 20°. If we assume that the errors have a normal distribution and less than 1% fall outside of the angular resolution range, then the SNR has to reduce the standard deviation to less than 1/2.576 of 10°. That is, the SNR needs to be not less than −3 dB (at 3.90625 kHz) to realize the assumed precision. If less than 0.1% of the errors are to be out of the range, then the SNR should be at least 0 dB.

5.3   Power consumption

The power budget is a critical issue to be resolved in space missions. The allocation to each instrument depends on the spacecraft configuration. It is important to estimate the power consumption of the one-chip WPIA and its dependence on variations in its design.

The power consumption of the FPGA can be calculated using Xilinx Virtex-II Web Power Tool by inputing the number of logic gates and the system clock frequency. The power consumed by the FPGA is 410 mW with the one-chip WPIA configured by the "Waveform Calibration" containing two pairs of FFT-IFFT for three components of the waveforms, and the "Time Correction" with the allocation of 2048 words in the Block Select RAMs. The toggle rates are set to 20% and 5% for the "Waveform Calibration" and other components, respectively. These use a FFT data length of 1024 and a particle count rate of 10^5/s. In addition, one must take into account the power consumption of the three on-board FIFO memories, which is approximately 90 mW. Therefore, the total power of the one-chip WPIA is estimated to be 500 mW. Noting that the one-chip WPIA does not require other components such as a CPU or DSP,
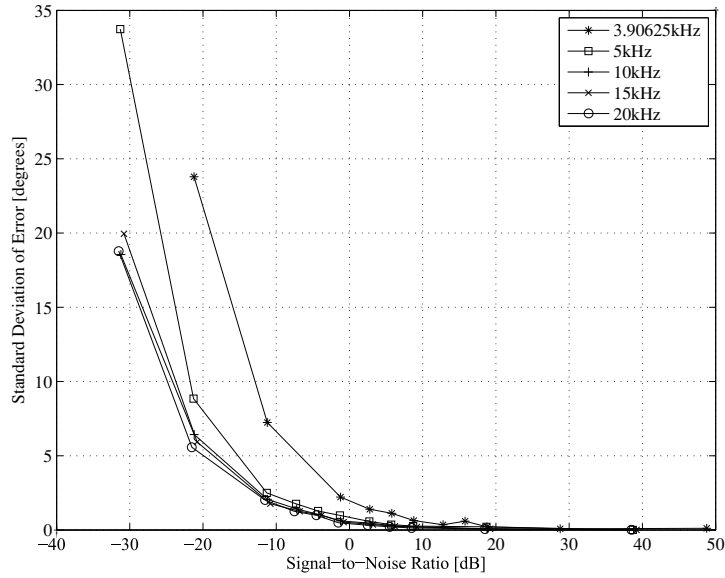
Fig. 19. Standard deviation of the errors in the "Waveform Calibration" are plotted against the signal-to-noise ratio at the frequencies of the input waveform of 3.90625 kHz, 5 kHz, 10 kHz, 15 kHz, and 20 kHz.

this total power consumption of 500 mW is feasible for the SCOPE mission.

6. Summary and Conclusion

Conventionally, the study of wave-particle interactions using observational data has been conducted by comparing the spectra of plasma waves with energy spectra or velocity distributions of plasmas. However, the relation between the phase and timing of the detected particles has been ignored, despite its importance in wave-particle interactions. Some attempts at directly measuring the wave-particle interactions have been made by rocket experiments and spacecraft observations (e.g., Ergun *et al.*, 1991; Kletzing *et al.*, 2005). They have focused on the relationship between the observed phase and the timing of the particle detections. However, since they counted particles by considering the observed wave phase, they did not obtain the physical energy flows. The WPIA provides $E_w \cdot v$, incorporating the time variation of the kinetic energies during the interactions of the waves and particles.

The calculation of $E_w \cdot v$ requires several procedures including waveform calibration and coordinate transformation. The waveform calibration is essential to obtain the correct phase from the observed data. The calibration consists of a calculation of the FFT and IFFT. It requires a dedicated digital processing component with high performance to accomplish real-time operation of the WPIA.

We succeeded in developing a new scientific instrument for studying wave-particle interactions in space. We called it the one-chip WPIA. It provides a solution for realizing the WPIA on a real-time basis with minimum resources. The one-chip WPIA is the FPGA which implements all of the necessary functions. The one-chip WPIA has been proposed for SCOPE (cross-Scale COupling in the Plasma universE) mission which targets the investigation of the cross-scale coupling in the terrestrial magnetosphere (SCOPE

working group, 2008). In the present paper, we demonstrated the design, functions, and performance of the one-chip WPIA. It consists of 4 blocks for individual functions of waveform calibration, coordinate transformation, time correction, and calculation of $E_w \cdot v$. These blocks operate in cooperation with other necessary sensors. Since the one-chip WPIA calculates $E_w \cdot v$ in reference to the ambient magnetic field, it needs data from the particle and magnetic field instruments as well as from the plasma wave receivers. The WPIA directs the processes in the above blocks by coordinating the data flows from these sensors.

We realized a one-chip WPIA on an evaluation board containing a plasma wave receiver and an interface with plasma instruments and other components needed in the development of the one-chip WPIA. By using this evaluation board, we confirmed that the one-chip WPIA works as designed. We showed that it continuously calculated $E_w \cdot v$ with enough precision and without delays.

Furthermore, we examined the accuracy of the waveform calibration by comparing the phase angles of the raw and calibrated waveforms. The accuracy was determined by the average and standard deviation of the error. The average and standard deviation explicitly increase when the SNR is smaller than 0 dB and 10 dB, respectively. Assuming an error range of $20°$ and a probability that the errors arising from the waveform calibration are out of range by 1% or 0.1%, a respective SNR of greater than -3 dB or 0 dB is required. Though the large errors at lower frequency have to be reduced by using several different numbers of FFTs or by setting a lower sampling frequency, we achieved good accuracy in the major range of frequency to be observed (several hundred Hz to around a dozen kHz) in the SCOPE mission.

The one-chip WPIA enables the study of various wave-particle interactions using spacecraft observation data. The power consumption is estimated to be 500 mW when

processing three components of waveforms sampled at 62.5 kHz and reading plasma data at a maximum count rate of 10^5/s. This specification is comparable to that of space missions for observing the terrestrial magnetosphere. Therefore, the one-chip WPIA is feasible for the SCOPE mission.

The most important feature of the one-chip WPIA is to guarantee real-time observations. Although the function of the one-chip WPIA can be realized by software running on a CPU, continuous operation in real time would be difficult. The software-type WPIA has been proposed for ERG (Energization and Radiation in Geospace), which is a small satellite mission focusing on the observation of the radiation belt of the Earth (ERG working group, 2008). On the other hand, a disadvantage of the one-chip WPIA compared to software WPIA is its smaller flexibility in the calculation and accumulation of $\boldsymbol{E}_{\mathrm{w}} \cdot \boldsymbol{v}$. For example, software WPIA can change accumulation procedures depending on the wave-particle interactions. We have not examined how much flexibility one can expect in a one-chip WPIA. Since there exist various types of wave-particle interactions in space, flexibility in the calculation and data accumulation is important. The next goal in the development of the one-chip WPIA is to incorporate as much flexibility as possible.

References

Buckley, A. M., M. P. Gough, H. Alleyne, K. Yearby, and I. Willis, Measurement of wave-particle interactions in the magnetosphere using the DWP particle correlator, *Proceedings of Cluster-II workshop*, 303–306, 2000.

Buckley, A. M., M. P. Gough, H. Alleyne, K. Yearby, and S. N. Walker, First measurements of electron modulations by the particle correlator expeiments on cluster, *Proceedings of the Les Woolliscroft Memorial Conference/Sheffield Space Plasma Meeting: Multipoint Measurements versus Theory, European Space Agency SP492*, 19–26, 2001.

ERG working group, Software-type wave-particle interaction analyzer, Proposal of the ERG mission, 62–65, Japan Aerospace Exploration Agency, 2008 (in Japanese, submitted).

Ergun, R. E., C. W. Carlson, J. P. McFadden, J. H. Clemmons, and M. H. Boehm, Langmuir wave growth and electron bunching: Results from a wave-particle correlator, *J. Geophys. Res.*, **96**, 225–238, 1991.

Ergun, R. E., J. P. McFadden, and C. W. Carlson, Wave-particle correlator instrument design, in *Measurement Techniques in Space Plasmas: Particles*, AGU, Geophysical Monograph 102, 325–331, 1998.

Gough, M. P., Particle correlator instruments in space: Performance; limitation, successes, and the future, in *Measurement Techniques in Space Plasmas: Particles*, AGU, Geophysical Monograph 102, 333–338, 1998.

Gough, M. P., D. A. Hardy, M. R. Oberhardt, W. J. Burke, L. C. Gentile, B. McNeil, K. Bounar, D. C. Thompson, and W. J. Raitt, Correlator measurements of megahertz wave-particle interactions during electron beam operations on STS, *J. Geophys. Res.*, **100**(A11), 21,561–21,575, 1995.

Kletzing, C. A., S. R. Bounds, J. Labelle, and M. Samara, Observation of the reactive component of Langmuir wave phase bunched electrons, *Geophys. Res. Lett.*, **43**, doi:10.1029/2004GL021175, 2005.

Matsumoto, H., H. Kojima, T. Miyatake, Y. Omura, M. Okada, I. Nagano, and M. Tsutsui, Electrostatic solitary waves (ESW) in the magnetotail: BEN wave forms observed by GEOTAIL, *Geophys. Res. Lett.*, **21**, 2915–2918, 1994a.

Matsumoto, H., I. Nagano, R. R. Anderson, H. Kojima, K. Hashimoto, M. Tsutsui, T. Okada, I. Kimura, Y. Omura, and M. Okada, Plasma wave observations with GEOTAIL spacecraft, *J. Geomag. Geoelectr.*, **46**, 59–95, 1994b.

SCOPE working group, One-chip wave-particle interaction analyzer, Proposal of the SCOPE mission, 449–458, Japan Aerospace Exploration Agency, 2008 (in Japanese, submitted).

H. Fukuhara (e-mail: fukuhara@rish.kyoto-u.ac.jp), H. Kojima, Y. Ueda, Y. Omura, Y. Katoh, and H. Yamakawa